

Molecular Weaving of Covalent Organic Frameworks for Adaptive Guest Inclusion

Yuzhong Liu,[†] Yanhang Ma,[‡] Jingjing Yang,[†] Christian S. Diercks,[†] Nobumichi Tamura,[§] Fangying Jin,[†] and Omar M. Yaghi^{*,†}

[†]Department of Chemistry, University of California—Berkeley, and Materials Sciences Division, Lawrence Berkeley National Laboratory, Kavli Energy NanoSciences Institute, Berkeley, California 94720, United States

[‡]School of Physical Science and Technology, Shanghai Tech University, Shanghai 201210, China

[§]Advanced Light Source, Lawrence Berkeley National Laboratory, Berkeley, California 94720, United States

Supporting Information

ABSTRACT: The synthesis of new isorecticular non-interpenetrated woven covalent organic frameworks (COFs) was achieved by linking aldehyde-functionalized copper(I) bisphenanthroline complexes with benzidine linkers in the presence of a bulky anion, diphenylphosphinate (PO_2Ph_2^-) to give metalated COF-506-Cu and, upon removal of copper(I), the demetalated COF-506. The structures of these COFs were determined by a combination of powder X-ray diffraction and electron microscopy techniques. Guest-accessibility to the pores of the two frameworks was examined by vapor and dye inclusion studies and compared to the already reported doubly-interpenetrated COF-505-Cu. Remarkably, COF-506 was found to take up guest molecules that exceed the size of the COF-506-Cu pores, thus giving credence to the notion of a novel mode of motional dynamics in solids we term ‘adaptive inclusion’.

Relative to dynamics observed in discrete molecules, extended solids are commonly perceived as being non-dynamic. With the advent of reticular chemistry, it has become possible to introduce motions into solids by using flexible building blocks^{1–3} and dangling switchable^{4–6} or mechanically interlocked units^{7,8} into the pores (Scheme 1a–c). In this Communication, we introduce a fourth scenario made possible by molecular weaving of covalent organic frameworks (COFs), where threads of covalently bonded organic molecules are interlaced at regular intervals to form two- and three-dimensional COFs.^{9–12} The fact that the interactions between the threads are mechanical in nature and therefore much weaker relative to those covalent bonds within the threads, allows collective large-amplitude movements with respect to each other. Openness within woven constructs facilitates these movements, while the interlacing prevents unzipping and ensures the fidelity of the overall system. These properties, especially the ease with which movement of the threads can be achieved, are ideally suited for woven frameworks to adapt to variously shaped incoming guests thus giving rise to ‘adaptive dynamics’ (Scheme 1d). In biological systems, adaptive binding is commonly credited for combining selectivity with maximizing substrate–host interactions to affect highly specific

functions. Adaptive dynamics in these COFs, being reliant on mechanical interlacing of threads as described in here, forgoes the need to stretch and bend chemical bonds throughout an extended structure to achieve collective motion.

The first generation of woven COFs were found to be dense structures with little internal guest-accessible void space.^{9,10} This posed an intrinsic limitation to the COF’s dynamic behavior as the openness of woven constructs dictates the magnitude of their dynamic motion. Here, we report the synthesis and crystal structures of a new isorecticular woven metalated COF-506-Cu (Scheme 2), and porosity studies done on COF-506-Cu and its demetalated form COF-506. We also use our previously reported COF-505-Cu as a reference point to evaluate the effects of pore size and degrees of interpenetration on the dynamics of these woven frameworks. The crystal structure of COF-506-Cu was determined by a combined transmission electron microscopy (TEM), 3D electron diffraction tomography (3D-EDT), and powder X-ray diffraction (PXRD) approach. Vapor and dye inclusion in these structures is studied to probe the porosity and capability to exhibit adaptive dynamics.

Designed Synthesis and Characterization of COF-506-Cu. We previously reported the design and synthesis of the first woven framework, COF-505-Cu, using an aldehyde-functionalized $\text{Cu}(\text{PDB})_2\text{BF}_4$ complex as the tetrahedral building block, which was reticulated with a linear ditopic benzidine (BZ) linker to yield a 2-fold interpenetrated 3D framework with an underlying dia topology (Scheme 2a). dia nets are self-dual and, as such, prone to self-interpenetration.¹³ In the case of COF-505-Cu, this limited the available internal space and restricted the dynamic motion of the threads. To avoid interpenetration during framework formation and maximize the guest accessible void space, a bulky anion (PO_2Ph_2^- , diphenylphosphinate) was used to occupy the internal voids in COF-506-Cu. The anions are then post-synthetically exchanged with BF_4^- to obtain more spacious pores (Scheme 2b).

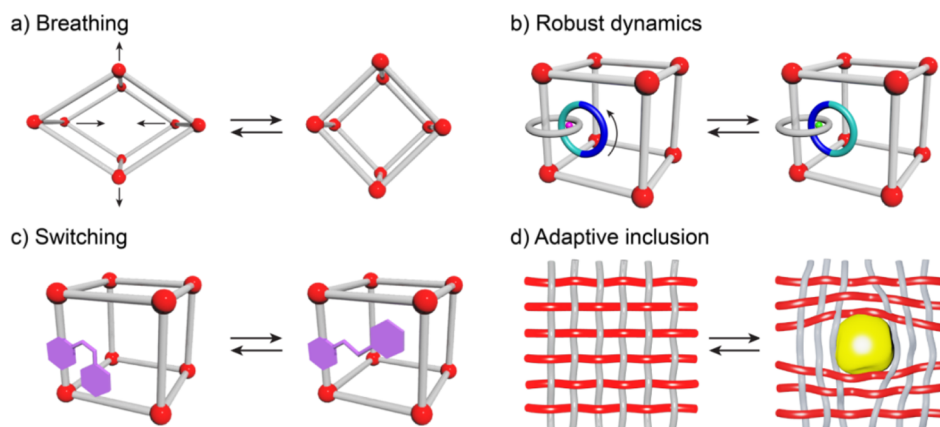
COF-506-Cu was synthesized under solvothermal conditions (Supporting Information (SI), Section S2). Completion of the reaction was confirmed by Fourier-transform

Received: August 20, 2018

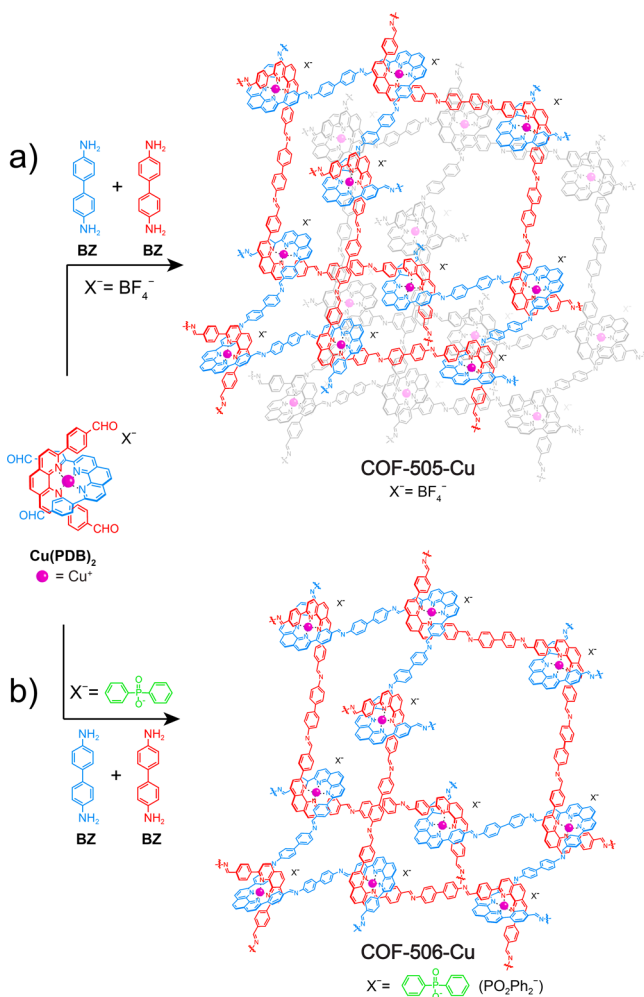
Published: October 1, 2018



Scheme 1. Modes of Dynamics in Solids: (a) Flexible Constituents Yield Frameworks That Distort in Response to External Stimuli, (b) Mechanically Interlocked Molecules (Blue and Green) Appended onto the Struts Move within the Constraints Imposed by Their Interlocking, (c) Switchable Units (Purple) Dangling in the Pores Respond to External Stimuli by Conformational Changes, and (d) Woven Frameworks Where Large Degrees of Freedom of the Threads Allow for Adaptive Inclusion of Guests (Yellow).



Scheme 2. Synthetic Scheme for the Formation of Doubly-interpenetrated COF-505-Cu and the Woven Non-interpenetrated COF-506-Cu



infrared spectroscopy (FT-IR), where the emergence of a peak at 1623 cm^{-1} (Figures S2–S4, 1622 cm^{-1} for COF-505-Cu) was assigned to the characteristic C=N stretching mode of

formed imine bonds. Successful post-synthetic anion exchange of COF-506-Cu was confirmed by the presence of a prominent band at 1057 cm^{-1} , assigned to the asymmetric stretching mode of BF_4^- .¹⁴ Furthermore, the ^1H NMR spectrum of acid-digested COF shows an equimolar ratio of the starting materials (PDB vs BZ), confirming completion of the COF-forming imine condensation reaction (SI, Section S5).

Structure Determination of COF-506-Cu. The morphology and purity of the as-synthesized material were examined by scanning electron microscopy (SEM), where a single phase of rod-shaped crystals several micrometers in length (Figure 1a) was observed. One single crystal (Figure 1b inset) was then chosen for 3D-EDT.¹⁵ A data set was collected (Figure 1b) by combining specimen tilt and electron-beam tilt in the range from -30.2° to $+41.2^\circ$, with a beam-tilt step of 0.2° . The 3D reciprocal lattice of COF-506-Cu was constructed and identified as a monoclinic Bravais lattice with unit cell parameters of $a = 27.7\text{ \AA}$, $b = 21.9\text{ \AA}$, $c = 33.8\text{ \AA}$, $\beta = 104^\circ$, and $V = 19895\text{ \AA}^3$, which were further refined to be $a = 27.0\text{ \AA}$, $b = 23.1\text{ \AA}$, $c = 34.6\text{ \AA}$, $\beta = 108^\circ$, and $V = 20533\text{ \AA}^3$ by Pawley refinement against the experimental PXRD pattern. High-resolution transmission electron microscopy (HRTEM) images viewed from the [010] and [100] directions show ordered lattice fringes, and the resultant fast Fourier diffractogram (FD) matches well with the experimental data set of the 3D-EDT (Figure 1c,d). According to these parameters, a structure model of COF-506-Cu was constructed in the monoclinic space group Pc (SI, Section S7).¹⁶ The calculated PXRD pattern of the modeled structure was found to be in good agreement with the experimental pattern of activated COF-506-Cu (Figure 1e).

In the crystal structure of the woven COF-506-Cu, tetrapotic $\text{Cu}(\text{PDB})_2$ constituents are linked by linear ditopic BZ to yield a framework with underlying **dia** topology (Figure 2). COF-506-Cu consists of chemically identical polyimine helices with a pitch of 14.1 \AA that propagate along the [110] and $[-110]$ directions (highlighted in blue and red) to construct a 3D pore system with the largest channels of $11.1\text{ \AA} \times 15.2\text{ \AA}$ running along the crystallographic b direction.

THF Vapor Adsorption and Dye Inclusion Studies. To test whether the pore space of the woven COF-506-Cu and the reported COF-505-Cu are guest-accessible, the structures were

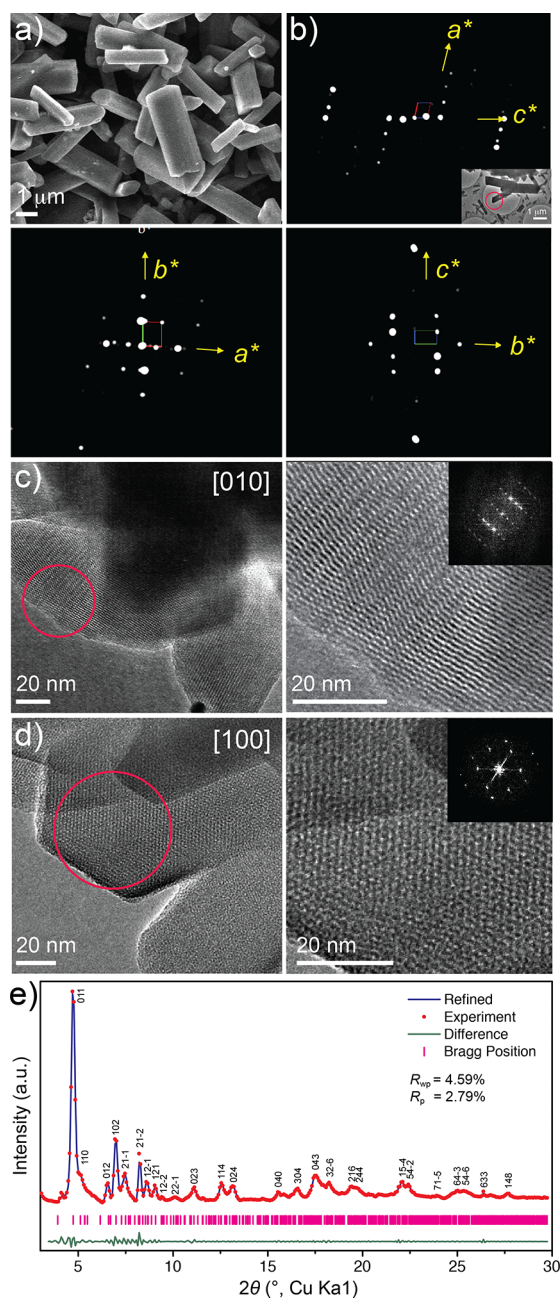


Figure 1. Electron microscopy and X-ray diffraction studies of COF-506-Cu. (a) SEM shows rod-shaped single crystals of COF-506-Cu. (b) 2D projection of the reconstructed reciprocal lattice of COF-506-Cu obtained from 3D-EDT data. Inset: TEM image of the single crystal used for 3D-EDT. (c,d) HRTEM images of COF-506-Cu taken with [010] and [100] incidence and magnified views of the circled areas with FD (inset) are in good agreement with the experimental measurements in (b). (e) Indexed PXRD pattern of activated COF-506-Cu (red, PO_2Ph_2^- counteranions) and Pawley refinement (blue) against the modeled structure. The pattern does not change upon anion exchange with BF_4^- . The difference plot and calculated Bragg positions are highlighted in green and pink, respectively.

examined by tetrahydrofuran (THF) vapor adsorption (SI, Section S8). COF-505-Cu shows a negligible uptake of THF, which is attributed to the relatively small pores that are occupied by solvated BF_4^- anions. In contrast, COF-506-Cu exhibits an isotherm with a major uptake at low partial pressure

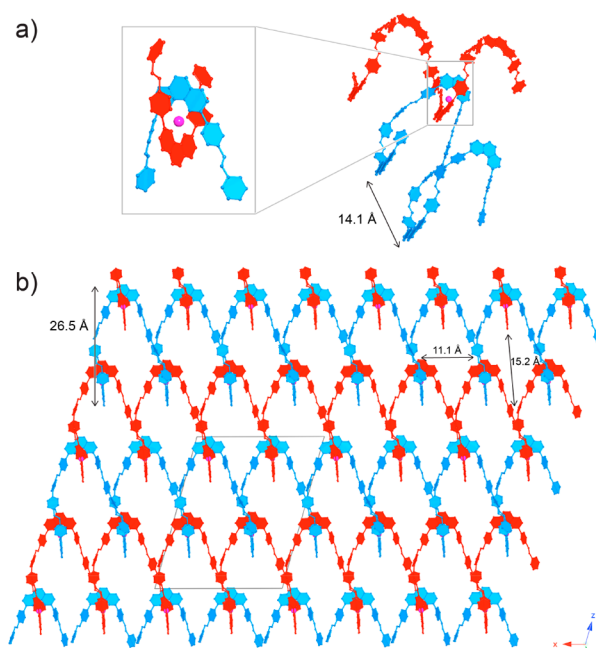


Figure 2. Crystal structure of woven COF-506-Cu. (a) COF-506-Cu consists of 1D helices with a pitch of 14.1 Å. (b) Helices highlighted in blue and red propagate in the [110] and [−110] directions, respectively, with copper(I) ions (pink) serving as points of registry. Neighboring blue and red helices are woven to form the overall framework viewed along the b axis. All hydrogen atoms are omitted for clarity.

indicative of a microporous material. The first step in the isotherm is reached at $P/P_0 = 0.2$ with $39.6 \text{ cm}^3 \text{ g}^{-1}$, and the maximum uptake reached $56.6 \text{ cm}^3 \text{ g}^{-1}$ at $P/P_0 = 0.98$ (SI, Section S8).

Furthermore, inclusion studies with anionic fluorescent dyes^{17–19} of increasing sizes [methyl orange (MO) < hydroxynaphthol blue disodium salt (HN) < methyl blue (MB)] were employed to evaluate the dimensions of the guest-accessible pores (Figure 3a–c). Five mg of activated COF were immersed in a 100 ppm methanol solution containing the guest compound to be included. The amount of molecules in the supernatant was measured using ultraviolet–visible (UV–vis) spectrophotometry, and the characteristic absorbance at 432 nm (MO), 540 nm (HN), or 606 nm (MB) was monitored over a period of 3 h. Owing to the positively charged framework backbone, the uptake of the anionic dyes can be attributed to a combination of adsorption and anion exchange. Nevertheless, it provides insight into the accessible pore dimensions of the frameworks. The results are plotted in Figure 3, and clearly show a continuous decrease of the amount of MO in the supernatant in the presence of COF-506-Cu, while only a negligible amount of inclusion was observed for COF-505-Cu (SI, Section S9). As the size of the dye increases, a significant amount of HN was only adsorbed by COF-506-Cu. Finally, in the case of MB, both frameworks did not display any major uptake. In summary, the pore dimensions increase significantly from COF-505-Cu to COF-506-Cu, in good agreement with their respective pore sizes obtained from the crystal structures.

Demetalation of COF-506-Cu and Dye Adaptive Inclusion in COF-506. The copper(I) ions in COF-506-Cu were removed to obtain the demetalated woven form, COF-506. This was affected by heating the framework in a 1 M

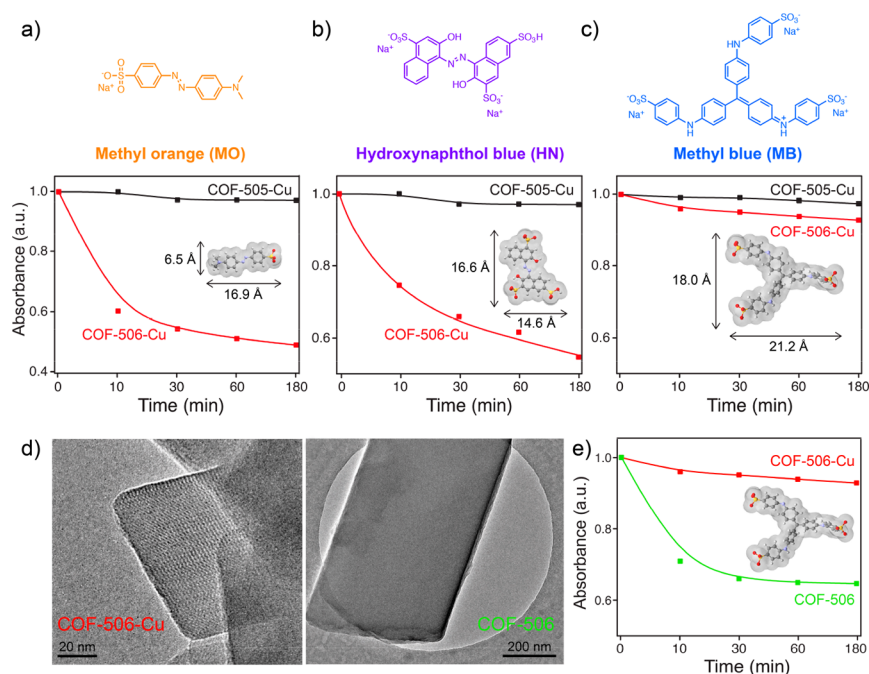


Figure 3. Inclusion studies of COF-505-Cu (black), COF-506-Cu (red), and COF-506 (green) with anionic dye molecules: (a) methyl orange (MO), (b) hydroxynaphthol blue (HN), and (c) methyl blue (MB). (d) TEM images of COF-506-Cu and COF-506. Upon demetalation, the lattice fringes indicative of the framework's crystalline nature disappeared, while the morphology of the single crystal was retained. (e) MB uptake of COF-506 compared to COF-506-Cu.

KCN methanol solution at 75 °C yielding COF-506. Inductively coupled plasma atomic emission spectroscopy analysis revealed that 99% of the copper ions were removed. Under the same conditions, COF-505-Cu could not be demetalated due to limited accessibility of its internal surface. Upon demetalation, the drastically decreased crystallinity of COF-506 and the disappearance of lattice fringes in the TEM micrographs (Figure 3d) indicate motional dynamics of the threads within the structure and therefore loss of long-range periodicity as such motions are non-coordinated. In contrast, the morphology of the crystals remained unaffected which is attributed to the fact that the overall connectivity of the structure is retained and threads remain interlaced and unzipped. This is corroborated by the fact that the chemical integrity of the structure was maintained: The FT-IR imine stretching vibration at 1623 cm^{-1} in COF-506 is identical to the one of its metalated progenitor (SI, Section S10).

The inclusion of MB dye in COF-506 shows a major uptake, 11.6-fold higher than that of its metalated analogue (Figure 3e). Upon demetalation, the absence of copper(I) ions allows the threads to move about in order to adapt and accommodate the inclusion of dye molecules that otherwise cannot fit within the original metalated form. It should be noted that the higher uptake cannot be rationalized by the absence of counterions in the pores since these would be exchanged by the negatively charged dye. As such, anisotropic structural rearrangements are necessary to open up the framework, thereby adapting to accommodate the MB dye guests.

■ ASSOCIATED CONTENT

📄 Supporting Information

The Supporting Information is available free of charge on the ACS Publications website at DOI: 10.1021/jacs.8b08949.

Synthetic protocols, PXRD analysis, structural modeling, and details on vapor as well as dye inclusion studies, including Figures S1–S14 and Tables S1–S4 (PDF)

■ AUTHOR INFORMATION

Corresponding Author

*yaghi@berkeley.edu

ORCID

Yuzhong Liu: 0000-0001-5614-1951

Jingjing Yang: 0000-0002-1192-7368

Christian S. Diercks: 0000-0002-7813-0302

Omar M. Yaghi: 0000-0002-5611-3325

Notes

The authors declare no competing financial interest.

■ ACKNOWLEDGMENTS

The crystal structure of $\text{Cu}(\text{PDB})_2\text{PO}_2\text{Ph}_2$ is available from the Cambridge Crystallographic Data Centre under the reference number CCDC-1870357. Financial support for COF research in the O.M.Y. laboratory was provided by KACST through the Joint UC Berkeley-KACST Center of Excellence for Nanomaterials for Clean Energy Applications, King Abdulaziz City for Science and Technology. Y.L. was supported by the Philomathia Graduate Student Fellowship in the Environmental Sciences. Y.M. acknowledges funding support from National Science Foundation of China (NSFC grant no. 21875140). C.S.D. would like to acknowledge the Kavli foundation for funding through a Kavli ENSI graduate student fellowship. The Advanced Light Source is supported by the Director, Office of Science, Office of Basic Energy Sciences, of the U.S. Department of Energy under Contract No. DE-AC02-05CH11231. The authors acknowledge Dr. Zheng Liu for

HRTEM data requisition, Xiaokun Pei and Dr. Eugene A. Kapustin for help with XRD.

■ REFERENCES

- (1) Serre, C.; Millange, F.; Thouvenot, C.; Noguès, M.; Marsolier, G.; Louër, D.; Férey, G. *J. Am. Chem. Soc.* **2002**, *124*, 13519–13526.
- (2) Férey, G.; Serre, C. *Chem. Soc. Rev.* **2009**, *38*, 1380–1399.
- (3) Krause, S.; Bon, V.; Senkovska, I.; Stoeck, U.; Wallacher, D.; Töbrens, D. M.; Zander, S.; Pillai, R. S.; Maurin, G.; Coudert, F.-X.; Kaskel, S. *Nature* **2016**, *532*, 348–352.
- (4) Brown, J. W.; Henderson, B. L.; Kiesz, M. D.; Whalley, A. C.; Morris, W.; Grunder, S.; Deng, H.; Furukawa, H.; Zink, J. I.; Stoddart, J. F.; Yaghi, O. M. *Chem. Sci.* **2013**, *4*, 2858–2864.
- (5) Schneemann, A.; Bon, V.; Schwedler, I.; Senkovska, I.; Kaskel, S.; Fischer, R. A. *Chem. Soc. Rev.* **2014**, *43*, 6062–6096.
- (6) Horike, S.; Shimomura, S.; Kitagawa, S. *Nat. Chem.* **2009**, *1*, 695–704.
- (7) Zhao, Y. L.; Liu, L.; Zhang, W.; Sue, C. H.; Li, Q.; Miljanić, O. Š.; Yaghi, O. M.; Stoddart, J. F. *Chem. - Eur. J.* **2009**, *15*, 13356–13380.
- (8) Deng, H.; Olson, M. A.; Stoddart, J. F.; Yaghi, O. M. *Nat. Chem.* **2010**, *2*, 439–443.
- (9) Liu, Y.; Ma, Y.; Zhao, Y.; Sun, X.; Gandara, F.; Furukawa, H.; Liu, Z.; Zhu, H.; Zhu, C.; Suenaga, K.; Oleynikov, P.; Alshammari, A. S.; Zhang, X.; Terasaki, O.; Yaghi, O. M. *Science* **2016**, *351*, 365–369.
- (10) Zhao, Y.; Guo, L.; Gandara, F.; Ma, Y.; Liu, Z.; Zhu, C.; Lyu, H.; Trickett, C. A.; Kapustin, E. A.; Terasaki, O.; Yaghi, O. M. *J. Am. Chem. Soc.* **2017**, *139*, 13166–13172.
- (11) Liu, Y.; O’Keeffe, M.; Treacy, M. M. J.; Yaghi, O. M. *Chem. Soc. Rev.* **2018**, *47*, 4642–4664.
- (12) Liu, Y.; Yaghi, O. M. *Bull. Jpn. Coord. Chem.* **2018**, *71*, 12–17.
- (13) Friedrichs, O. D.; O’Keeffe, M.; Yaghi, O. M. *Solid State Sci.* **2003**, *5*, 73–78.
- (14) Heimer, N. E.; Del Sesto, R. E.; Meng, Z.; Wilkes, J. S.; Carper, W. R. *J. Mol. Liq.* **2006**, *124*, 84–95.
- (15) Gemmi, M.; Oleynikov, P. Z. *Kristallogr. - Cryst. Mater.* **2013**, *228*, 51–58.
- (16) Dassault Systèmes BIOVIA. *Materials Studio 8.0*; Dassault Systèmes, San Diego, CA, 2014.
- (17) Ning, G. H.; Chen, Z.; Gao, Q.; Tang, W.; Chen, Z.; Liu, C.; Tian, B.; Li, X.; Loh, K. P. *J. Am. Chem. Soc.* **2017**, *139*, 8897–8904.
- (18) Fang, Q.; Zhuang, Z.; Gu, S.; Kaspar, R. B.; Zheng, J.; Wang, J.; Qiu, S.; Yan, Y. *Nat. Commun.* **2014**, *5*, 4503.
- (19) Haque, E.; Jun, J. W.; Jhung, S. H. *J. Hazard. Mater.* **2011**, *185*, 507–511.

■ NOTE ADDED AFTER ASAP PUBLICATION

Changes were made on October 12, 2018.